Princeton Plasma Physics Laboratory

PPPL-4125
PPPL-4125

The Effect of Plasma Shaping on Performance in the National Spherical Torus Experiment (NSTX)

D.A. Gates, R. Maingi, J. Menard, S. Kaye,
S.A. Sabbagh, G. Taylor, J.R. Wilson,
et al.

November 2005

Prepared for the U.S. Department of Energy under Contract DE-AC02-76CH03073.

The effect of plasma shaping on performance in the National Spherical Torus Experiment (NSTX)

D. A. Gates[1], R. Maingi[4], J. Menard[1], S. Kaye[1], S.A. Sabbagh[2], G. Taylor[1], J.R. Wilson[1], M.G. Bell[1], R.E. Bell[1], S. Bernabei[1], J. Bialek[2], T. Biewer[1], W. Blanchard[1], J. Boedo[3], C. Bush[4], M.D. Carter[4], W. Choe[5], N. Crocker[6], D.S. Darrow[1], W. Davis[1], L. Delgado-Aparicio[7], S. Diem[1], J. Ferron[8], A. Field[9], J. Foley[1], E.D. Fredrickson[1], T. Gibney[1], R. Harvey[10], R.E. Hatcher[1], W. Heidbrink[11], K. Hill[1], J.C. Hosea[1], T.R. Jarboe[12], D.W. Johnson[1], R. Kaita[1], C. Kessel[1], S. Kubota[6], H.W. Kugel[1], J. Lawson[1], B.P. LeBlanc[1], K.C. Lee[13], F. Levinton[14], J. Manickam[1], R. Maqueda[14], R. Marsala[1], D. Mastrovito[1], T.K. Mau[3], S.S. Medley[1], H. Meyer[9], D.R. Mikkelsen[1], D. Mueller[1], T. Munsat[15], B.A. Nelson[12], C. Neumeyer[1], N. Nishino[16], M. Ono[1], H. Park[1], W. Park[1], S. Paul[1], W. Peebles[6], M. Peng[4], C. Phillips[1], A. Pigarov[3], R. Pinsker[8], A. Ram[17], S. Ramakrishnan[1], R. Raman[12], D. Rasmussen[4], M. Redi[1], M. Rensink[18], G. Rewoldt[1], J. Robinson[1], P. Roney[1], L. Roquemore[1], E. Ruskov[11], P. Ryan[4], H. Schneider[1], C.H. Skinner[1], D.R. Smith[1], A. Sontag[2], V. Soukhanovskii[18], T. Stevenson[1], D. Stotler[1], B. Stratton[1], D. Stutman[7], D. Swain[4], E. Synakowski[1], Y. Takase[19], K. Tritz[7], A. von Halle[1],

M. Wade[4], R. White[1], J. Wilgen[4], M. Williams[1], W. Zhu[2], S.J. Zweben[1],

R. Akers[9], P. Beiersdorfer[18], R. Betti[20], T. Bigelow[4]

[1]*Princeton Plasma Physics Laboratory, Princeton University, Princeton, NJ 08543, USA*
[2]*Dept. of Applied Physics, Columbia Univ., NYC, NY, USA*
[3]*University of California, San Diego, CA, USA*
[4]*Oak Ridge National Laboratory, Oak Ridge, TN, USA*
[5]*Korea Advanced Institute of Science and Technology, Taejon, Republic of Korea*
[6]*University of California, Los Angeles, CA, USA*
[7]*Johns Hopkins University, Baltimore, MD, USA*
[8]*General Atomics, San Diego, CA, USA*
[9]*Euratom-UKAEA Fusion Associates, Abingdon, Oxfordshire, UK*
[10]*CompX, Del Mar, CA, USA*
[11]*University of California, Irvine, CA, USA*
[12]*University of Washington, Seattle, WA, USA*
[13]*University of California, Davis, CA, USA*
[14]*Nova Photonics, Princeton, NJ, USA*
[15]*University of Colorado, Boulder, CO, USA*
[16]*Hiroshima University, Hiroshima, Japan*
[17]*Massachusetts Institute of Technology, Cambridge, MA, USA*
[18]*Lawrence Livermore National Laboratory, Livermore, CA, USA*
[19]*Tokyo University, Tokyo, Japan*
[20]*University of Rochester, Rochester, NY, USA*

Abstract

NSTX has explored the effects of shaping on plasma performance as determined by many diverse topics including: the stability of global MHD modes (e.g. ideal external kinks and resistive wall modes), Edge Localized Modes (ELMs), bootstrap current drive, divertor flux expansion, and heat transport. Improved shaping capability has been crucial to achieving $\beta_t \sim 40\%$. Precise plasma shape control has been achieved on NSTX using real-time equilibrium reconstruction. NSTX has simultaneously achieved elongation $\kappa \sim 2.8$ and triangularity $\delta \sim 0.8$. Ideal MHD theory predicts increased stability at high values of shaping factor $S \equiv q_{95}I_p/(aB_t)$, which has been observed at large values of the $S \sim 37[MA/(m \cdot Tesla)]$ on NSTX. ELM behavior is observed to depend on plasma shape. A description of the ELM regimes attained as shape is varied will be presented. Increased shaping is predicted to increase the bootstrap fraction at fixed I_p. The achievement of strong shaping, has enabled operation with 1s pulses with I_p = 1MA, and for 1.6s for $I_p = 700kA$. Analysis of the non-inductive current fraction as well as empirical analysis of the achievable plasma pulse length as elongation is varied will be presented. Data is presented showing a reduction in peak divertor heat load due

to increasing in flux expansion.

1 Introduction

The spherical torus is currently being studied as a potential path to the development of fusion energy at reduced capital cost and as a potential low cost neutron source for materials testing. In addition, the study of plasmas at low aspect-ratio enables the investigation of plasma physics in fusion relevant plasma regimes outside the normal operational parameter space of conventional tokamaks and thereby expands the range over which the theories which predict plasma performance can be tested. Reactor studies, such as the ARIES-ST study [1], have shown that, in order to achieve the desired high bootstrap current fraction necessary for economical operation of an ST, it is required to operate with strong plasma shaping. Similar studies for neutron sources, such as the Component Test Facility (CTF) [2], also require more shaping than has been maintained in steady state in any existing device. In addition, Edge Localized Modes are a serious issue for the proposed ITER device, and the stability of these modes depends on plasma shape. This paper reports on efforts made on the National Spherical Torus Experiment to investigate the performance of plasmas that approach the shaping requirements of ST conceptual designs and to investigate the physics of plasma shaping.

2 Machine Improvements

In order to better investigate strongly shaped plasmas, several improvements to the shape control capabilities of NSTX have been made. These improvements were required in order to overcome the the difficulties associated with maintaining shaped plasmas in steady state. In particular, changes were made that addressed the need to control the n=0 vertical instability at high elongation, the need to provide X-point control at high triangularity, and the ability to maintain constant shape as well as make fine scale shape adjustments during a discharge.

The primary method by which vertical instability control was improved was through a reduction in the latency of the control system. The control system on NSTX is a digital computer based system which acquires 352 channels of data in real-time and controls the magnet power supplies and the plasma fueling [3, 4]. The control system latency is the time between when a disturbance is sensed in the plasma and the time when corrective action is taken. The mean latency in the NSTX control system was measured to be $3ms$ before the upgrades were performed. Both hardware and software optimizations were performed (each of which roughly equally improved the system latency) with a final measured latency of $0.75ms$. The results of this improvement are summarized in Figure 1, which shows the achieved plasma elongation ($\kappa \equiv b/a$, where b is half the vertical extent of the plasma and a is half of the radial extent) as a function of the normalized internal inductance, l_i. The dependence of the instability vertical growth rate on elongation and normalized internal inductance is well documented (see e.g. reference [5]). Each point in the figure represents one EFIT reconstruction from the NSTX database. The data has been sorted to remove plasmas with excessive vertical motion on a time scale typical of vertical instability on NSTX. The red points in the figure are from discharges made before the latency reduction, while the green points are from after the reduction. For fixed l_i, the maximum achievable elongation increased by 20-30%.

In order to achieve increased plasma triangularity, $\delta(\equiv [R_{top} - R_{cent}]/a)$ where R_{top} is the major radius of the uppermost point on the plasma boundary, R_{cent} is the geometric center of the plasma, and a is the plasma geometric minor radius) simultaneous with high κ, it was necessary to modify the poloidal field coil arrangement on NSTX. Figure 2 shows the changes made to the PF1A poloidal field coils, which are located at the ends of the central solenoid. The height of the coil was reduced to $\sim 1/2$ the original height. This allows formation of an X-point on the inboard side of the plasma near the top of the vacuum vessel. Also shown in Figure 2 are example double-null divertor equilibria, one from before and one from after the PF1A coil upgrade. The change in the achievable triangularity is apparent.

In addition to these changes, rtEFIT/isoflux control [6] of the plasma boundary has been implemented on NSTX. rtEFIT was first used on NSTX in 2003 [7] and has been used to control plasmas heated by radio frequency waves for which accurate control of the gap between the plasma and the RF antenna is needed. Improvements to the accuracy and speed of the real-time equilibrium reconstructions have extended the utility of rtEFIT/isoflux control to the highest performance plasmas on NSTX. In fact, the longest 1MA discharge ever run on NSTX was made using the rtEFIT/isoflux control algorithm. Data from such a discharge is shown in Figure 3, which has a sustained β_t for $\sim 2\tau_R$. The implementation of rtEFIT has also enabled several detailed shape variation experiments that have offered insight in to the behavior of ELMs. These experiments will be described briefly in section 5.

3 Global Performance Improvements

Two of the major benefits that are associated with increased plasma shaping are an increase in the achievable β_t and increased bootstrap fraction, f_{bs}. The effect of plasma shaping on β_t is presented in Figure 4, which shows the flat-top averaged β_t plotted against the plasma current flat-top time for the same shot. Each point in this plot represents one NSTX plasma discharge. The data are also sorted by plasma shaping factor S [$\equiv q_{95}I_p/(aB_t)[MA/(m \cdot Tesla)]$, where q_{95} is the safety factor on the 95% flux surface] with color corresponding to shape factor. As is evident from the figure, increasing the shape factor has increased both pulse length at fixed β_t and β_t at fixed pulse length.

To understand the benefit of increased shaping more fully, we define a figure of merit, $\beta_{sus} \equiv f_{bs}\beta_t \sim C_{bs}\sqrt{\epsilon}\beta_p\beta_t \sim C_{bs}\sqrt{\epsilon}(1+\kappa^2)/2(\beta_N/2)^2$, where $C_{bs} \sim 0.5$ is the coefficient which approximately relates the bootstrap fraction to $\sqrt{\epsilon}\beta_p$ and where use has been made of an elliptical approximation for the plasma boundary. This figure of merit, which has been previously identified in reference [8], has the benefit that it balances the inherent trade-off between β_t and bootstrap fraction (and hence pulse length) that is apparent in Figure 4. To verify the general scaling of the relationship between approximate relationship given above, we plot $\sqrt{\epsilon}\beta_p\beta_t$ versus $1+\kappa^2$ in Figure 5. As in Figure 1, red points are for time before the control system upgrade and green is after. The data in Figure 5 are averaged over the plasma current flat-top, so each point represents one NSTX discharge. Separate analysis of the validity of the approximate expression $f_{bs} \sim \sqrt{\epsilon}\beta_p$ has been performed using the TRANSP code with a smaller database and the relationship is valid within $10-20\%$. The deviation between the approximation and the TRANSP calculated value of the bootstrap current can be attributed to the fast particle pressure in the plasma, which does not contribute to the bootstrap current, but which does contribute to total pressure.

4 Long Pulse Discharges

As a result of plasma shaping, NSTX has been able to operate with longer pulse length. In particular, discharges with pulse lengths of $\sim 1.6s$ have been achieved. This corresponds to $\sim 50\tau_E$, where τ_E is the energy confinement time and more importantly, to $\sim 6\tau_R$ where $\tau_R \equiv \mu_0\sigma_{NC}a^2/6$ is the resistive diffusion time for the first radial moment of the current profile [9] with $\sigma_{NC} \sim 2R_0(I_p - I_{non-inductive})/(V_{loop}a^2\kappa)$ is the neoclassical electrical conductivity.

These discharges have high non-inductive current fractions of $\sim 60\%$, with $\sim 85\%$ of the non-inductive current being due to pressure driven currents. The non-inductive current fraction in this case consists of the sum of the neutral beam driven current, the bootstrap current, the diamagnetic current, and the Pfirsch-Schluter current divided by the total plasma current. Figure 6 shows the time history of the non-inductive current fraction as well as other plasma parameters for such a long pulse discharge. The normalized β, $\beta_N (\equiv \beta_t a B_t / I_p)$ is calculated to be well above the no-wall limit of $\beta_N \sim 4$ for the first 1s of the pulse, until the onset of a large $n = 1$ mode that reduces the confinement of both the thermal plasma as well as the fast ions that heat the plasma. An interesting aspect of this particular discharge is that the pulse length is determined by the thermal limits of the toroidal field coil rather than instabilities or the available flux in the ohmic transformer.

5 ELM Characteristics

An important aspect of plasma performance that is associated with changes in plasma shaping is the behavior of Edge Localized Modes (ELMs). The ELM characteristics of lower triangularity high elongation long pulse discharges from the 2004 run (see, e.g., Reference [10]) were not optimal, in that the ELMS from these discharges were large and had a measurable impact on the global energy confinement time. Long pulse discharges from 2005, which were run using the modified PF1A coils and had higher triangularity, had substantially improved ELM characteristics. The ELMs were smaller and, as a result, confinement was improved. Figure 7 shows a comparison between shot 112581 from 2004 and 117707 from 2005 demonstrating this change in ELM regime. Unfortunately, since there was not a controlled experiment to systematically vary the plasma boundary in the long-pulse regime, it is difficult to conclude definitively that the shape changes are responsible for the change in ELM behavior. Other changes to discharge conditions, such as the differing beam power or different vessel wall conditions may also be responsible for the observed changes.

A systematic experiment was peformed to examine the effect on ELM behavior of changing the divertor configuration from lower single-null through balanced double-null to an upper single null. Similar experiments have been performed in the past to look at the H-mode power threshold [11] This change is characterized by the δr_{sep} shape parameter defined as the distance between the flux surfaces which pass through the X-points as measured at the outboard mid-plane. This study was carried out using the rtEFIT/isoflux shape control algorithm. This experiment demonstrated that small changes to the plasma boundary can indeed influence the ELM behavior in a dramatic way. δr_{sep} was systematically varied over between +2mm to -2mm (positive δr_{sep} corresponds to an upper single-null and negative to lower single-null). Lower single-null plasmas had substantially smaller ELMs and exhibited energy confinement times $\sim$ 1.5 times higher than upper single-null plasmas. The characteristics of these small ELMs are described in Reference [12]. This change in ELM behavior was reproducible over several shots. An example of consecutive shots with otherwise fixed parameters is shown in Figure 8. The plasma boundaries are overlayed for comparison. Also shown in the Figure 9 are the time histories of δr_{sep} as determined from equilibrium reconstructions. Note the scale of variation is in mm. This experiment demonstrates the power of precision boundary control in creating new research opportunities, which in turn can offer greater insight into the physics of ELMs. ELMs have been shown to be a crucial issue for ITER [13] and other future burning plasma experiments.

6 Divertor Power Loading

Controlling peak heat flux is a critical issue for ITER and other burning plasma experiments, including potential future ST experiments. An additional benefit of high triangularity at low aspect ratio is strong divertor flux expansion. In lower flux expansion regimes, the divertor power loading on NSTX is similar to that expected for ITER as first shown in [14]. Figure 10 shows the effect of varying plasma shape on divertor power loading. Each shot in the figure has identical heating power, but by changing from low triangularity $\delta \sim 0.4$ single-null to low triangularity double-null to high triangularity $\delta \sim 0.8$ double-null, the peak heat flux is successively reduced from $\sim 10\mathrm{MW/m^2}$ to $\sim 5\mathrm{MW/m^2}$ to $\sim 2.5\mathrm{MW/m^2}$. The ability to study heat flows in varying divertor geometries is a powerful tool for understanding the impact of flux expansion on peak heat flux.

7 Summary

As expected, plasma shape has had a substantial impact on plasma performance on NSTX. The topics discussed in the current paper, namely β-limits, plasma pulse length, bootstrap current fraction, ELM behavior, and divertor power loading, are just a subset of the important physics issues that are affected by the shape of the plasma boundary. Boundary shape control has the distinct benefit of being an existing field of study with precise tools and detailed theories available to compare to experiment. Understanding the effect of plasma shaping in regimes that have not yet been explored represents a prime opportunity to validate and expand the utility of these theories in ways that are not possible in conventional operational regimes.

This work was supported by the U.S. Department of Energy Grant under contract number DE-AC02-76CH03073.

References

[1] F. Najmabadi and the ARIES Team, Fusion Engineering and Design, **65** (2003) 143

[2] M. Peng, et al., to be published Plasma Physics and Controlled Fusion (2006)

[3] D. A. Gates, D. Mueller, C. Neumeyer, J. R. Ferron, IEEE Trans. on Nucl. Sci. **47** (2000) 222, Part 1

[4] D. A. Gates, et al., to be published in Fus. Eng. Design (2006)

[5] F. Hofmann, et al., Nucl. Fusion **38** (1998) 1767

[6] J. R. Ferron, M. L. Walker, L. L. Lao, et al., Nucl. Fusion **38** 1055 (1998)

[7] D. A. Gates, to be published in Nucl. Fusion (2006)

[8] T. K. Mau, et al., Proceedings of the 18th IEEE/NPSS Symp. on Fusion Engineering, (Albuquerque, NM) 1999

[9] D. Mikkelson, Physics of Fluids B **1** (1989) 333

[10] S. Kaye, et al., Nucl. Fusion **45** (2005) S168.

[11] R. Maingi, et al., Nucl. Fusion **45** (2005) 245

[12] R. Maingi, et al., presented at this conference

[13] ITER Physics Basis Document, Chapter 3, Nucl.Fusion **39** (1999) 2251

[14] R. Maingi, Nucl. Fusion **43** (2003) 969

Figure Captions

Figure 1: Plasma elongation, $\kappa = b/a$ plotted versus normalized internal inductance, l_i for each EFIT reconstruction in the NSTX database, filtered against rapid vertical motion. The data in green is after the control system latency reduction.

Figure 2: The modification to the PF1A coil on NSTX has allowed simultaneous achievement of high κ and δ. The modified coil is shown on the right, and the original coil is shown on the left. Also shown are two typical high elongation double null plasmas produced using the different coils (shot 114465 on the left, 115911 on the right).

Figure 3: Plot showing the time dependence of current sources in shot 117707. The first frame shows TRANSP calculated values of the non-inductive current drive terms: the bootstrap current, the other pressure gradient driven currents (the diamagnetic and Pfirsch-Schluter currents), and the neutral beam driven current. The next 3 frames show the total plasma current, β_p as calculated by EFIT, and the total injected neutral beam power.

Figure 4: Each point in the above plot represents 1 discharge from the NSTX database. $< \beta_t >$ is β_t averaged over the plasma current flat-top and τ_{flat} is the flat-top time over which the average is performed. The data is binned by the plasma shaping factor $S \equiv q_{95} I_p/(aB_t)$ [MA/m·Tesla] and bins are marked with different colors as indicated in the plot legend. There is a strong correlation between increased shape factor and increased β_t and τ_{flat}.

Figure 5: Each point in the plot above represents one discharge in the NSTX database. The quantity $\sqrt{\epsilon}\beta_p\beta_t$ averaged over the plasma current flat-top is plotted against $1 + \kappa^2$, with κ also averaged over the current flat-top. The straight line in the curve is

meant only to guide the eye as an upper bound. The red points are from before the control system upgrade and the green points are from after.

Figure 6: Plot showing the time dependence of current sources in shot 116318. The first frame shows TRANSP calculated values of the non-inductive current drive terms: the bootstrap current, the other pressure gradient driven currents (the diamagnetic and Pfirsch-Schluter currents), and the neutral beam driven current. The next 3 frames show the total plasma current, β_p as calculated by EFIT, and the total injected neutral beam power.

Figure 7: Figure showing the time history of plasma parameters for shots 112581 from 2004 (black) and shot 117707 from 2005 (red). Note the dramatic change in ELM behavior.

Figure 8: Overlay of the plasma boundaries for shots 117424 (black, lower single null) and 117425 (red, upper single null).

Figure 9: The time history of plasma parameters for shots 117424 and 117425 (same shots as in Figure 8). The dramatic change in ELM behavior substantially changes the plasma performance. Also plotted is the parameter δr_{sep} in millimeters.

Figure 10: The peak heat flux versus major radius for three different divertor configurations: 1) low δ lower single null, 2) low δ double null, and 3) high $/delta$ double null. All three configurations had identical heating power. The peak heat flux reduces by a factor of ~ 5.

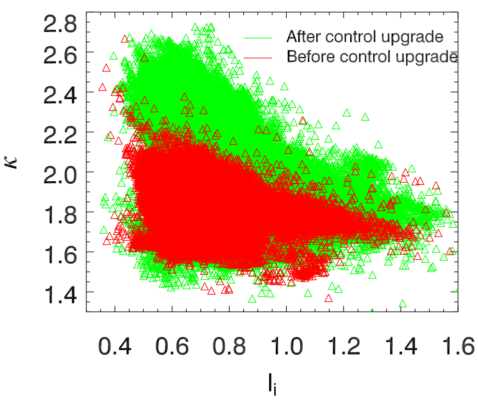
After control upgrade
Before control upgrade
2.8
2.6
2.4
2.2
2.0
1.8
1.6
1.4
0.4
0.6
0.8
1.0
1.2
1.4
1.6
κ
l_i

Figure 1:

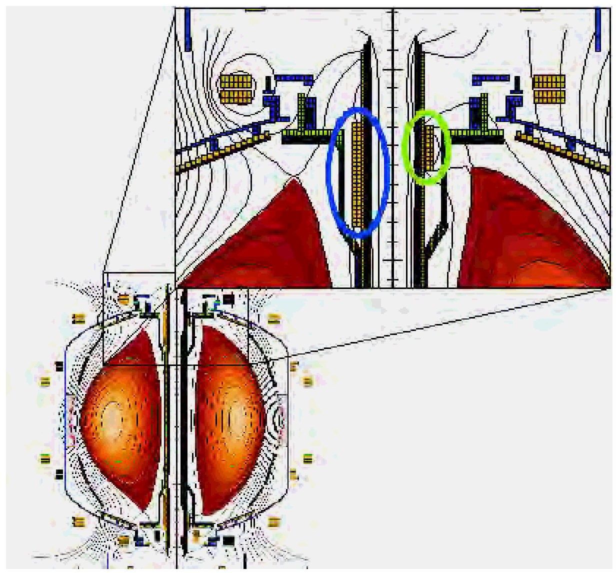

Figure 2:

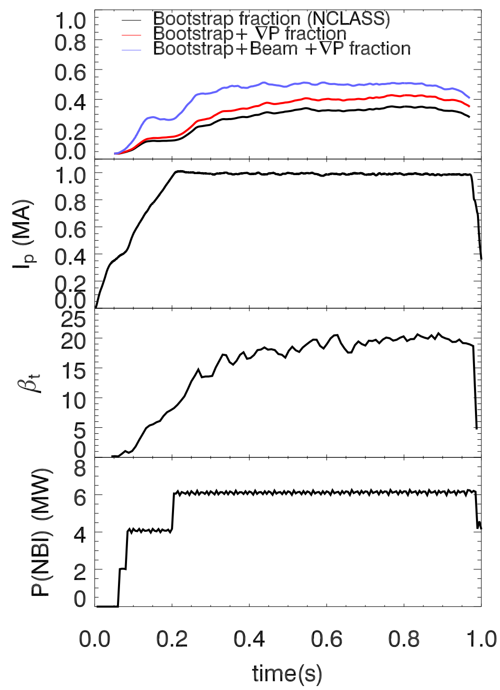
Bootstrap fraction (NCLASS)
Bootstrap+ ∇P fraction
Bootstrap+Beam +∇P fraction
1.0
0.8
0.6
0.4
0.2
0.0
I_p (MA)
1.0
0.8
0.6
0.4
0.2
0.0
β_t
25
20
15
10
5
0
P(NBI) (MW)
8
6
4
2
0
0.0
0.2
0.4
0.6
0.8
1.0
time(s)

Figure 3:

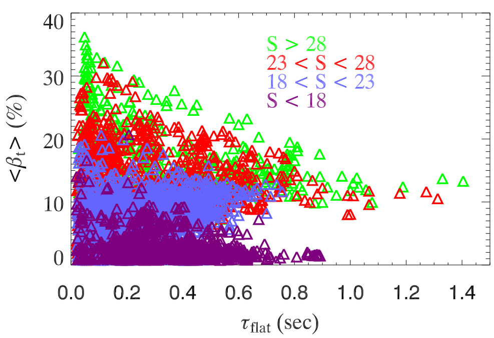

S > 28
23 < S < 28
18 < S < 23
S < 18
40
30
20
10
0
0.0
0.2
0.4
0.6
0.8
1.0
1.2
1.4
<β_t> (%)
$\tau_{\rm flat}$ (sec)

Figure 4:

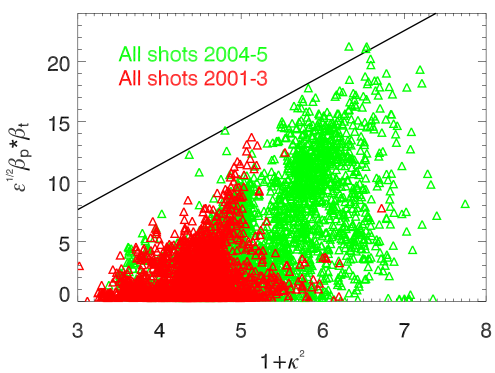

All shots 2004-5
All shots 2001-3
20
15
10
5
0
3
4
5
6
7
8
$\varepsilon^{1/2}\beta_p * \beta_t$
$1+\kappa^2$

Figure 5:

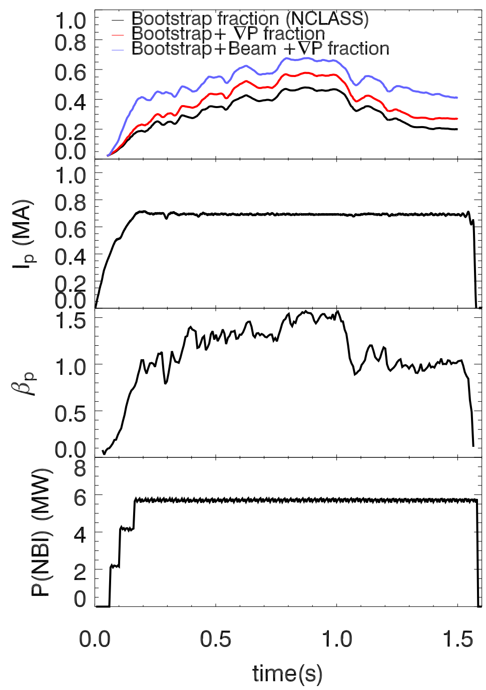

Bootstrap fraction (NCLASS)
Bootstrap+ ∇P fraction
Bootstrap+Beam +∇P fraction
1.0
0.8
0.6
0.4
0.2
0.0
I_p (MA)
β_p
1.5
1.0
0.5
P(NBI) (MW)
8
6
4
2
0
0.0
0.5
1.0
1.5
time(s)

Figure 6:

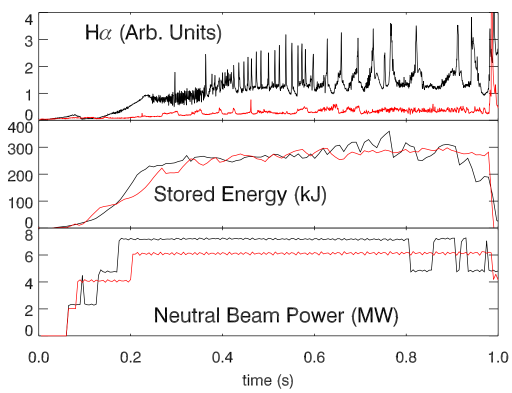

Figure 7:

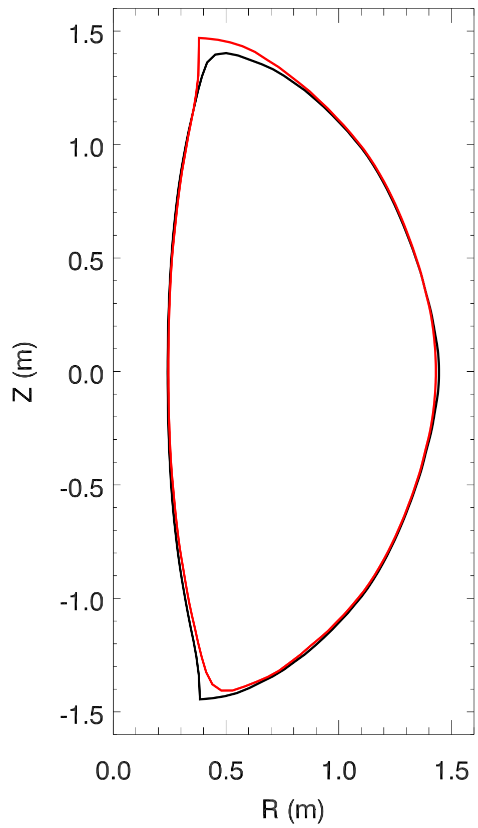

Figure 8:

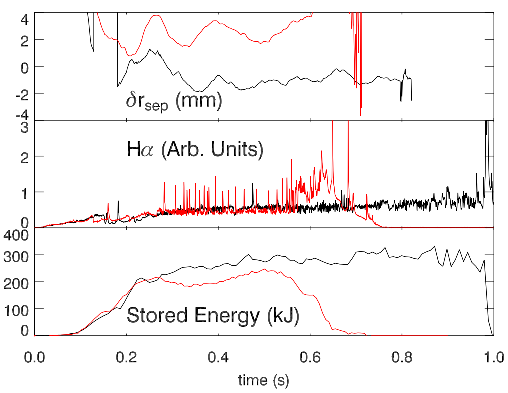

Figure 9:

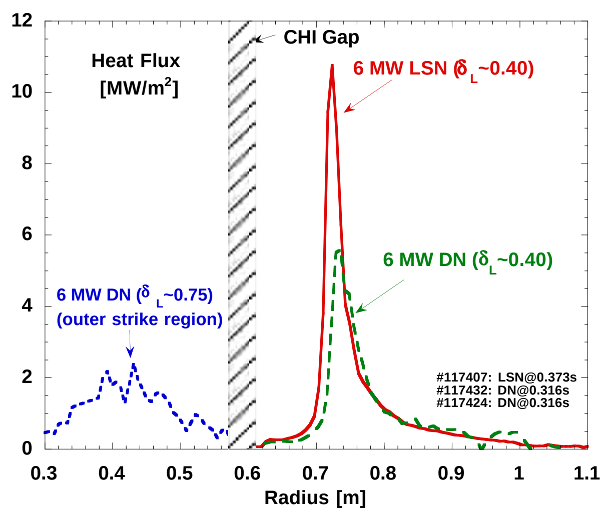

Heat Flux
[MW/m2]
CHI Gap
6 MW LSN (δ L~0.40)
6 MW DN (δ L~0.40)
6 MW DN (δ L~0.75)
(outer strike region)
#117407: LSN@0.373s
#117432: DN@0.316s
#117424: DN@0.316s
Radius [m]

Figure 10:

External Distribution

Plasma Research Laboratory, Australian National University, Australia
Professor I.R. Jones, Flinders University, Australia
Professor João Canalle, Instituto de Fisica DEQ/IF - UERJ, Brazil
Mr. Gerson O. Ludwig, Instituto Nacional de Pesquisas, Brazil
Dr. P.H. Sakanaka, Instituto Fisica, Brazil
The Librarian, Culham Science Center, England
Mrs. S.A. Hutchinson, JET Library, England
Professor M.N. Bussac, Ecole Polytechnique, France
Librarian, Max-Planck-Institut für Plasmaphysik, Germany
Jolan Moldvai, Reports Library, Hungarian Academy of Sciences, Central Research Institute for Physics, Hungary
Dr. P. Kaw, Institute for Plasma Research, India
Ms. P.J. Pathak, Librarian, Institute for Plasma Research, India
Dr. Pandji Triadyaksa, Fakultas MIPA Universitas Diponegoro, Indonesia
Professor Sami Cuperman, Plasma Physics Group, Tel Aviv University, Israel
Ms. Clelia De Palo, Associazione EURATOM-ENEA, Italy
Dr. G. Grosso, Instituto di Fisica del Plasma, Italy
Librarian, Naka Fusion Research Establishment, JAERI, Japan
Library, Laboratory for Complex Energy Processes, Institute for Advanced Study, Kyoto University, Japan
Research Information Center, National Institute for Fusion Science, Japan
Professor Toshitaka Idehara, Director, Research Center for Development of Far-Infrared Region, Fukui University, Japan
Dr. O. Mitarai, Kyushu Tokai University, Japan
Mr. Adefila Olumide, Ilorin, Kwara State, Nigeria
Dr. Jiangang Li, Institute of Plasma Physics, Chinese Academy of Sciences, People's Republic of China
Professor Yuping Huo, School of Physical Science and Technology, People's Republic of China
Library, Academia Sinica, Institute of Plasma Physics, People's Republic of China
Librarian, Institute of Physics, Chinese Academy of Sciences, People's Republic of China
Dr. S. Mirnov, TRINITI, Troitsk, Russian Federation, Russia
Dr. V.S. Strelkov, Kurchatov Institute, Russian Federation, Russia
Kazi Firoz, UPJS, Kosice, Slovakia
Professor Peter Lukac, Katedra Fyziky Plazmy MFF UK, Mlynska dolina F-2, Komenskeho Univerzita, SK-842 15 Bratislava, Slovakia
Dr. G.S. Lee, Korea Basic Science Institute, South Korea
Dr. Rasulkhozha S. Sharafiddinov, Theoretical Physics Division, Insitute of Nuclear Physics, Uzbekistan
Institute for Plasma Research, University of Maryland, USA
Librarian, Fusion Energy Division, Oak Ridge National Laboratory, USA
Librarian, Institute of Fusion Studies, University of Texas, USA
Librarian, Magnetic Fusion Program, Lawrence Livermore National Laboratory, USA
Library, General Atomics, USA
Plasma Physics Group, Fusion Energy Research Program, University of California at San Diego, USA
Plasma Physics Library, Columbia University, USA
Alkesh Punjabi, Center for Fusion Research and Training, Hampton University, USA
Dr. W.M. Stacey, Fusion Research Center, Georgia Institute of Technology, USA
Director, Research Division, OFES, Washington, D.C. 20585-1290

The Princeton Plasma Physics Laboratory is operated
by Princeton University under contract
with the U.S. Department of Energy.

Information Services
Princeton Plasma Physics Laboratory
P.O. Box 451
Princeton, NJ 08543

Phone: 609-243-2750
Fax: 609-243-2751
e-mail: pppl_info@pppl.gov
Internet Address: http://www.pppl.gov